Velocity tomography and reflectivity imaging using crosswell seismic data from the Noel tight gas field

Joe Wong and Robert R. Stewart

ABSTRACT

We analyze data from a crosswell seismic survey that was conducted in 2004 at the Noel gas field located in northeastern British Columbia and operated by BP Canada Energy Company. The goal was to create high-resolution images of gas-bearing, but tight, sandstone channels 2400 m to 2650 m deep in the Cadomin and Nikanassin formations. The survey employed hydrophones and a piezoelectric vibrator source operating between two wells approximately 145 m apart. The dominant frequencies in the crosswell seismograms are about 1.0 kHz to 1.5 kHz, with wavelengths on the order of 4 m to 6 m. Compared to wavelengths of about 100 m that are usual for surface seismic data, the shorter wavelengths in the crosswell data provide significantly better resolution of beds 10 m to 25 m thick. A P-wave velocity tomogram was created from first arrival times using a back-projection algorithm that accounts for head-wave arrivals. Wavefield separation isolated up-going and down-going reflections. These reflections were mapped with a VSP/CDP method that used ray-tracing guided by the velocity tomogram. Seismic boundaries on the velocity tomogram and the reflectivity image correlate closely with the known geology.

INTRODUCTION

The Noel Gas Field operated by BP Canada Energy Company is located in northeastern British Columbia. Tight, gas-bearing sandstone channels exist at depths of 2400 m to 2650 m. Gas production from these target zones may be stimulated by hydraulic fracturing. Before deciding whether or not to go forward with a hydraulic fracturing program, BP Canada wished to have more detailed information regarding the continuity of the sand channels. To this end, BP Canada contracted Z-Seis Corporation in 2004 to conduct high-resolution crosswell seismic survey between two wells, 00-A97-E and 02-A97-E. At the survey depths, the wells are separated by about 145 m.

Analysis of crosswell data usually involves two procedures: tomographic imaging of P-wave velocities using first-arrival times as input (Peterson et al., 1985; Wong et al., 1987), and mapping of observed reflections to create a reflectivity map (Stewart and Marchisio, 1991; Harris et al., 1995). In this study, we applied both techniques to obtain the seismic structure between the wells for comparison with the known geology.

Figure 1 shows the geological formations and boundaries encountered by the wells, along with the natural gamma-ray and P-wave sonic logs (the data on Figure 1 were provided by BP Canada Energy Limited). Low gamma activity and low transit times deflect to the left. Of primary interest is the Cadomin formation, described as sandstone and persistent sandy conglomerate. Below the Cadomin is the Nikanassin formation with the Monach, Beattie Peaks, and Monteith members. Zones where tight gas sand channels

exist, namely, the Cadomin, lower Monach, upper Monteith, and lower Monteith, have been colored in yellow. The remaining zones are largely shales and siltstones.
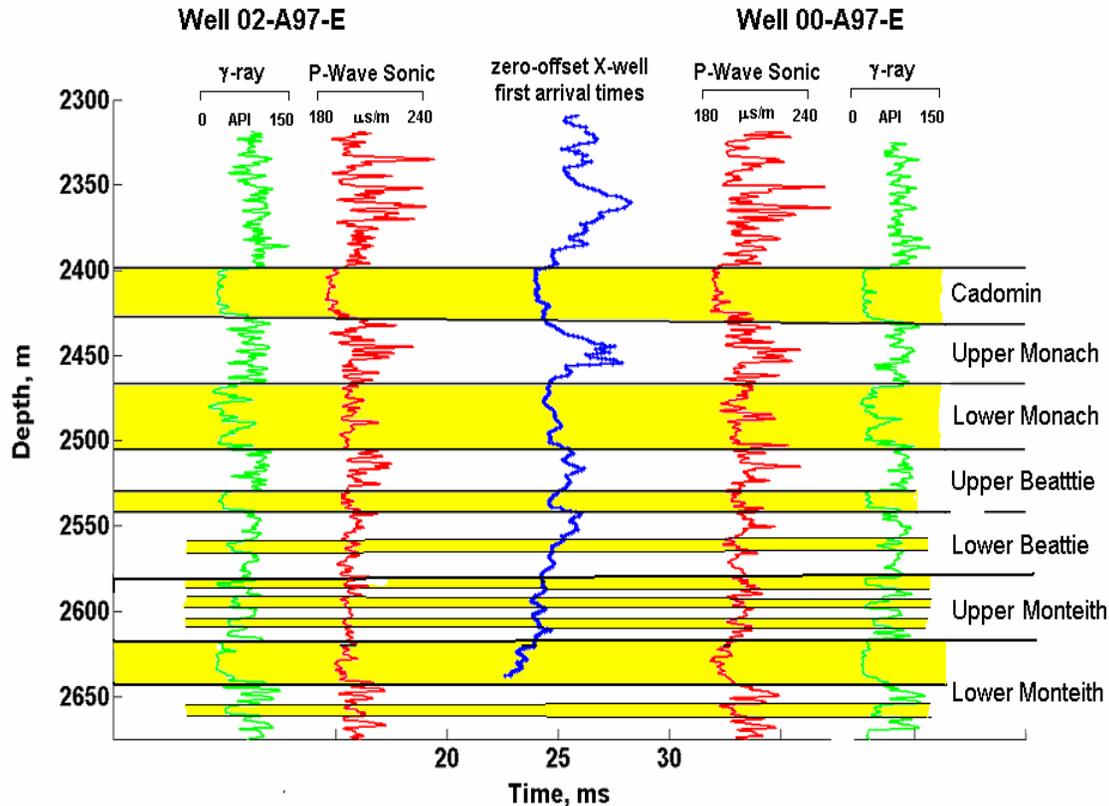

FIG. 1. Geology and geophysical logs in the Noel wells (gamma-ray and sonic data courtesy of BP Canada Energy Limited).

The natural gamma-ray logs closely follow the geology, with low activity coinciding with the sands in the Cadomin, lower Monach, upper Monteith, and lower Monteith. Higher gamma-ray activity in the other members is due to the presence of shales and siltstones. The gamma-ray logs delineate the geological boundaries with precision. The geological structure is essentially flat-lying.

The sonic logs, although rather noisy, also follow the geology. The sonic transit times in the shales and siltstones are on average larger than those in the sandstone formations. From the sonic log transit times, we find that the P-wave velocities are about 5.3 to 5.6 km/s in the sandstones, and about 4.5 to 5.0 km/s in the shales.

CROSSWELL SEISMIC ACQUISITION AND FIELD RESULTS

A piezoelectric vibrator controlled by a linear sweep was used as the source for the crosswell survey. The sweep was 1.1 seconds long, beginning at a low frequency of 100 Hz and ending at a high frequency of 2.0 kHz. The listen period was 1.6 seconds. The

digital sampling interval was .125 ms, resulting in a Nyquist frequency of 4.0 kHz. Raw field data, i.e., the pilot signal and the received signals, were recorded for post-acquisition crosscorrelation. During acquisition, an array of ten hydrophone receivers covered depths from 2300 m to 2650 m at 1.5 m intervals in Well 00-A97-E. The source occupied the same depth range at 0.75 m intervals in Well 02-A97-E. This procedure produced a dense network of more than 59,000 rays crossing the rock section. Figure 2 is a schematic diagram showing the crosswell scanning procedure for one common source gather. About 460 common source gathers and 230 common receiver gathers can be sorted from the 59,000 traces.
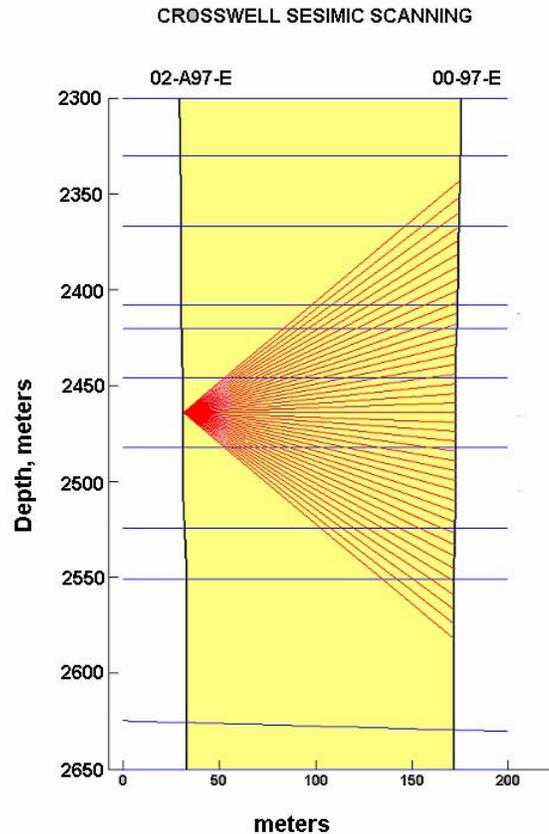

FIG. 2. Schematic diagram of crosswell scanning with the source in Well 02-A97-E, and receivers in Well 00-A97-E. The raypaths represent a common source gather.
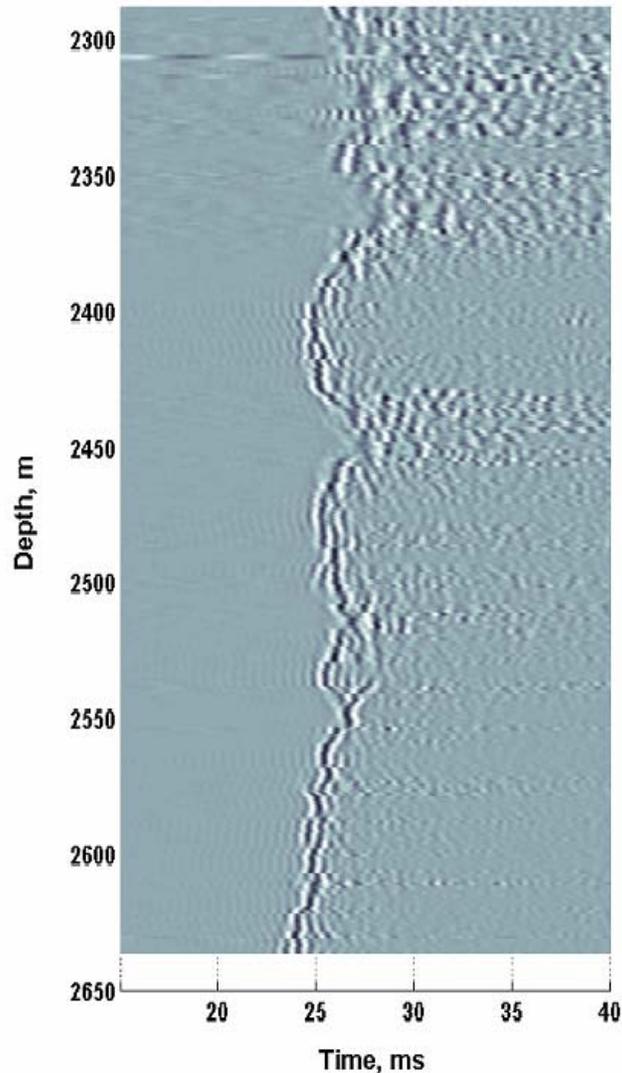
FIG. 3. Zero-offset (in depth) seismograms recorded with the piezoelectric source and hydrophone receivers.

Example seismic traces are shown on Figures 3 and 4. Figure 3 is a common depth or zero-offset gather, for which source and receiver depths are equal. Figure 4 is a common receiver gather with the receiver at a depth of 2484 m. The dominant frequencies on these seismograms are in the range 1.0 kHz to 1.5 kHz. We note the obvious variation of first arrival times with depth. We have picked the first arrival times on over 50,000 traces interactively, and have plotted the picks from the zero-offset gather on Figure 1 to emphasize their correlation with the geological formations. Fast arrivals are observed through the sandstone layers (low gamma-ray activity), while slower arrivals are associated with shales and siltstones (high gamma-ray activity).
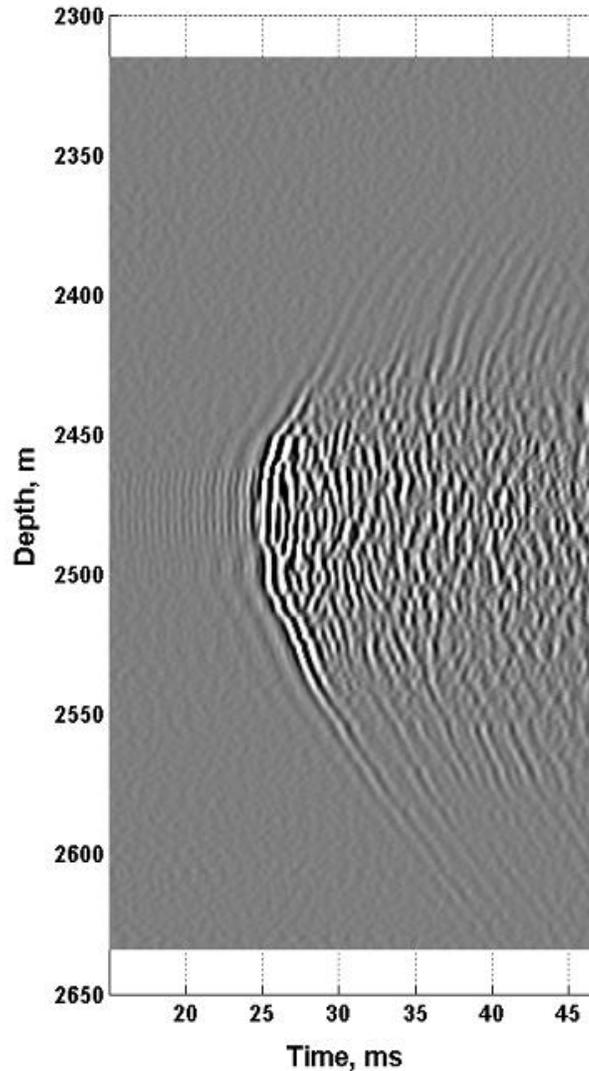
FIG. 4. Common receiver gather with receiver depth at 2484 m. Peak-to-peak times reveal a dominant frequency of about 1.0 to 1.5 kHz.

VELOCITY TOMOGRAM

For the flat, horizontally-layered geology, the main features of the seismic velocity structure in the rock section are determined by the first arrival times of the common depth (zero-offset) seismograms shown on Figure 3. Using a back-projection algorithm (Peterson et al., 1985), we created a P-wave velocity tomogram with first-arrival times from the zero-offset gather and gathers with source-receiver offsets of -50 m, -25 m, 25m, and 50 m. Imaging artifacts were eliminated by constraining the tomogram to have a flat, layered structure. Improved definition of boundaries between adjacent low- and high-velocity layers was achieved by carefully accounting for first arrival times from head waves.

In a low-velocity layer at locations close to the boundaries separating it from the higher-velocity zones above and below it, first arrival times will be from head waves that follow refracted trajectories through the higher-velocity zones. The corresponding arrival times are faster than if the paths had remained entirely within the low-velocity formations. If arrival times from these head waves are used in tomogram creation without consideration for this "speed-up" behavior, a bias is produced toward higher velocity values in the low-velocity zones. This bias causes a loss of contrast with the higher velocity zones above and below.
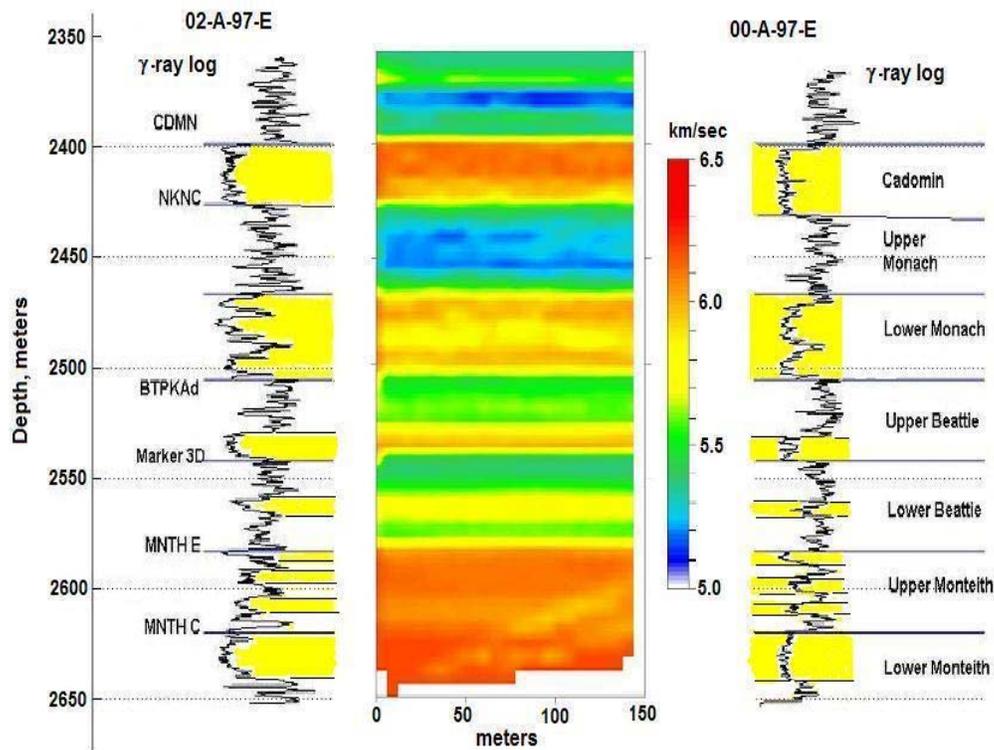

FIG. 5. P-wave velocity tomogram.

We can remove the bias and improve the contrast if, instead of using the first arrival times strictly, we identify the low-velocity zones (using the first-pass tomogram, natural gamma-ray logs, and the geology intersected by the wells) and make corrections to the zero-offset arrival times before a creating second-pass image. The corrections to the zero-offset arrival times through low-velocity zones are made in a way that is consistent with refraction into and out of the high-velocity zones above and below. A tomogram created with the corrected arrival times will then (1) account for refraction; (2) correlate better with known geology; (3) define geological boundaries more sharply; and (4) have more accurate velocity values.

Figure 5 shows the final P-wave velocity tomogram together with the gamma-ray logs and the geological formations. The tomogram clearly delineates the sandstones,

siltstones, and shales. Velocity values are in the range 5800 to 6200 m/sec for the sandstones and 5100 to 5500 m/s for the siltstones and shales.
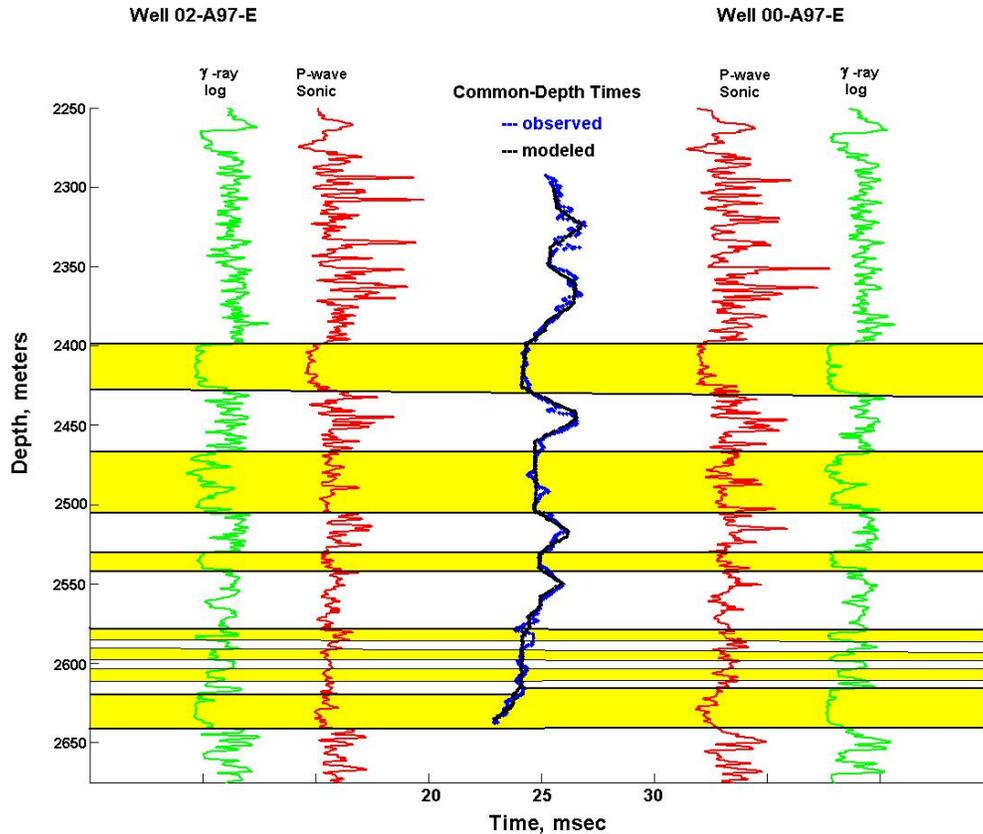

FIG. 6. Comparison between observed and calculate zero-offset first arrival times.

A comparison is shown on Figure 6 between the zero-offset first-break times picked from Figure 1 with first-break times calculated by ray-tracing direct and head-wave arrivals across the velocity model in Figure 5. The calculated times agree very well with the observed times.

REFLECTIVITY IMAGING

To produce a reflectivity map, we follow a procedure similar to those used by others (Stewart and Marchisio, 1991; Khalil et al., 1993; Lazaratos et al., 1995; Li and Stewart, 1996). The main steps in the processing flow are:

- sort to common source/receiver gathers;

- remove first arrivals to isolate reflections;

- F-K filtering for up-going reflections;

- F-K filtering for down-going reflections;

- VSP/CDP mapping of reflections;

- apply residual statics to align mapped reflections;

- stack the aligned reflections to obtain the final reflectivity image.

Figure 4 is an example of a common receiver gather. Following Lazaratos et al. (1995), we removed the first arrivals subtracting a running average (mean filtering). Alternatives that can be used to remove the first arrivals are median filtering and F-K filtering; however, in this case, the results are not overly sensitive to the specific method.

Figure 7 shows the up-going and down-going wavefields from Figure 4 after first arrival removal and velocity filtering in the F-K domain. These wavefields are dominated by P-P reflections. Weak events with larger near-linear moveout which may be P-S conversions are present in some, but not all, gathers. In this study, we will focus on only the P-P events. The up-going and down-going reflections are obtained from all the possible common receiver and common source gathers. The separated wavefields for every gather are then transformed by VSP/CDP mapping to yield partial reflectivity images. The VSP/CDP mapping technique (Wyatt and Wyatt, 1984) involves ray-tracing over a suitable velocity model (such as one in Figure 6 produced by velocity tomography) to find reflection locations in space for reflection events recorded in time.

Figure 8 shows examples of partial reflectivity maps. The left hand side is the partial reflectivity map of a single common receiver gather near the top of the crosswell panel. The right-sided-side is a sum of partial reflectivity maps from several gathers covering the entire depth extent of the panel. The reflecting boundaries are indicated by nearly horizontal features. However, the coherence and alignment are not particularly good.
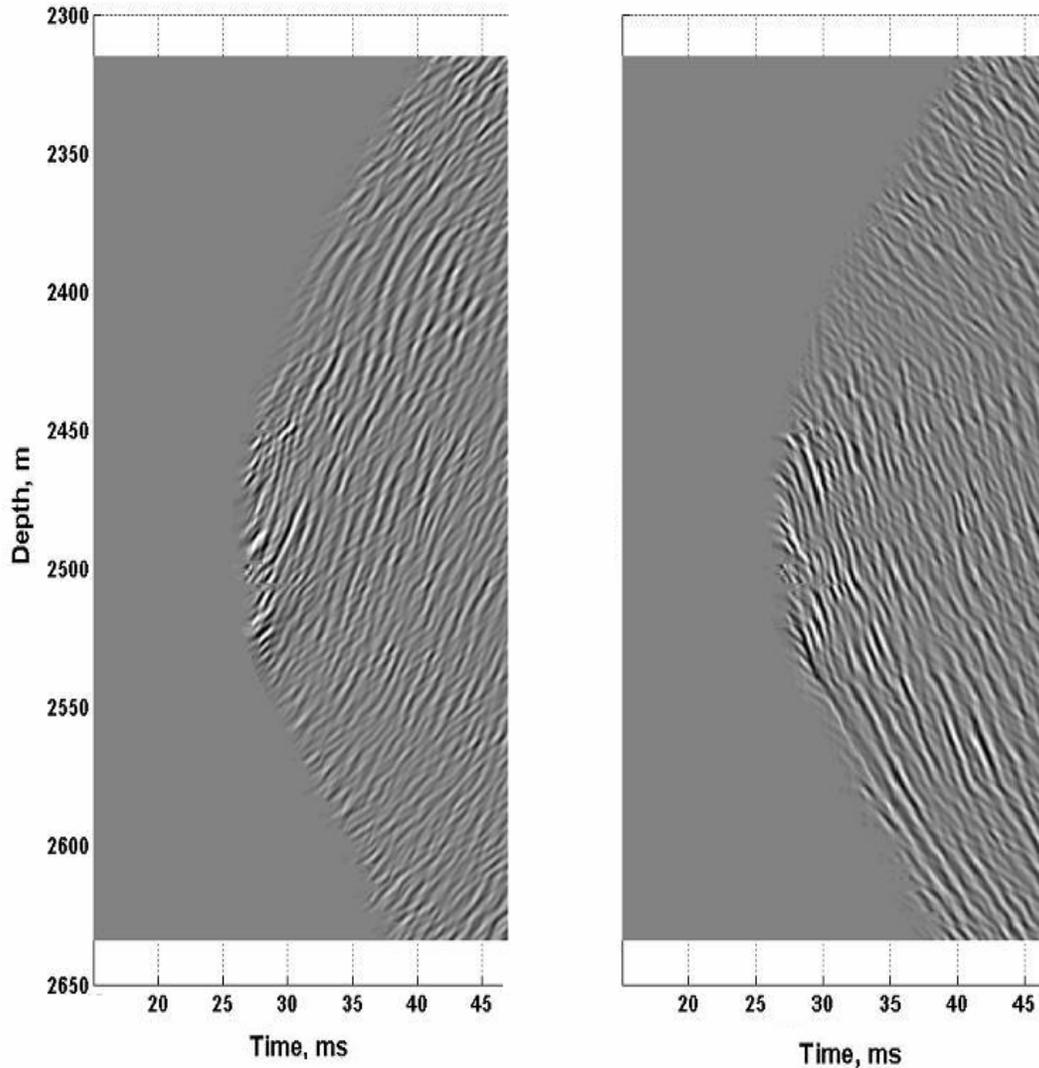
FIG. 7. Up-going and down-going wavefields from the gather in Figure 4.

    Lazaratos et al. (1995) have pointed out that the degradation in the coherence and alignment is due to the fact that ray-tracing cannot adequately account for complex effects such as lateral velocity variations, anisotropy, and mislocation of well trajectories. To account for these effects individually and deterministically is a complicated and time-consuming task.   Instead, we follow Lazaratos et al. (1995) and correct for all these effects by applying residual statics corrections to each major reflecting interface indicated by the velocity tomogram.   The result of applying statics corrections to the partial reflectivity maps on Figure 8 is shown on Figure 9. The improvement in both coherence and alignment of the mapped reflections is obvious.
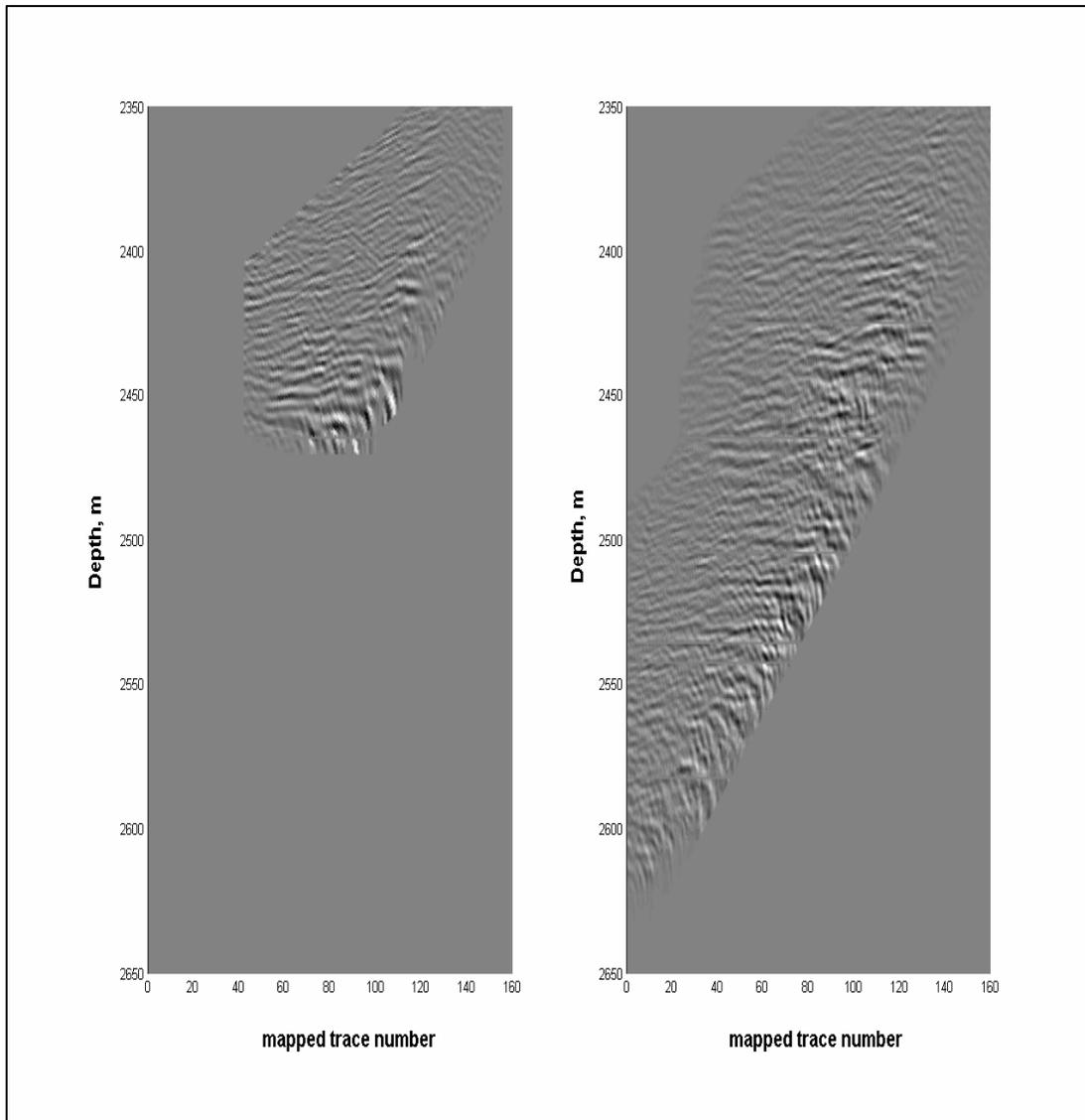
FIG. 8. Left: partial reflectivity map from a single common receiver gather. Right: stack of partial reflectivity maps from several common receiver gathers at different depths.

Even after residual statics corrections, distortions with low spatial frequencies remain near the edges of the partial reflectivity maps. These distortions are inherent to the VSP/CDP mapping procedure, and are caused by moveout stretch associated with raypaths that run nearly parallel to the reflecting horizons (Lazaratos et al., 1995). They are removed by transforming the partial reflection images to the vertical wavenumber domain and then applying a low-cut filter to remove low-wavenumber components. After transforming back to the space domain, the partial reflectivity maps associated with up-going and down-going wavefields on about 600 common receiver and common source gathers are stacked to produce the final image shown on Figure 10. The figure emphasizes the good agreement of the crosswell reflections with the known formation boundaries and the natural gamma-ray logs.
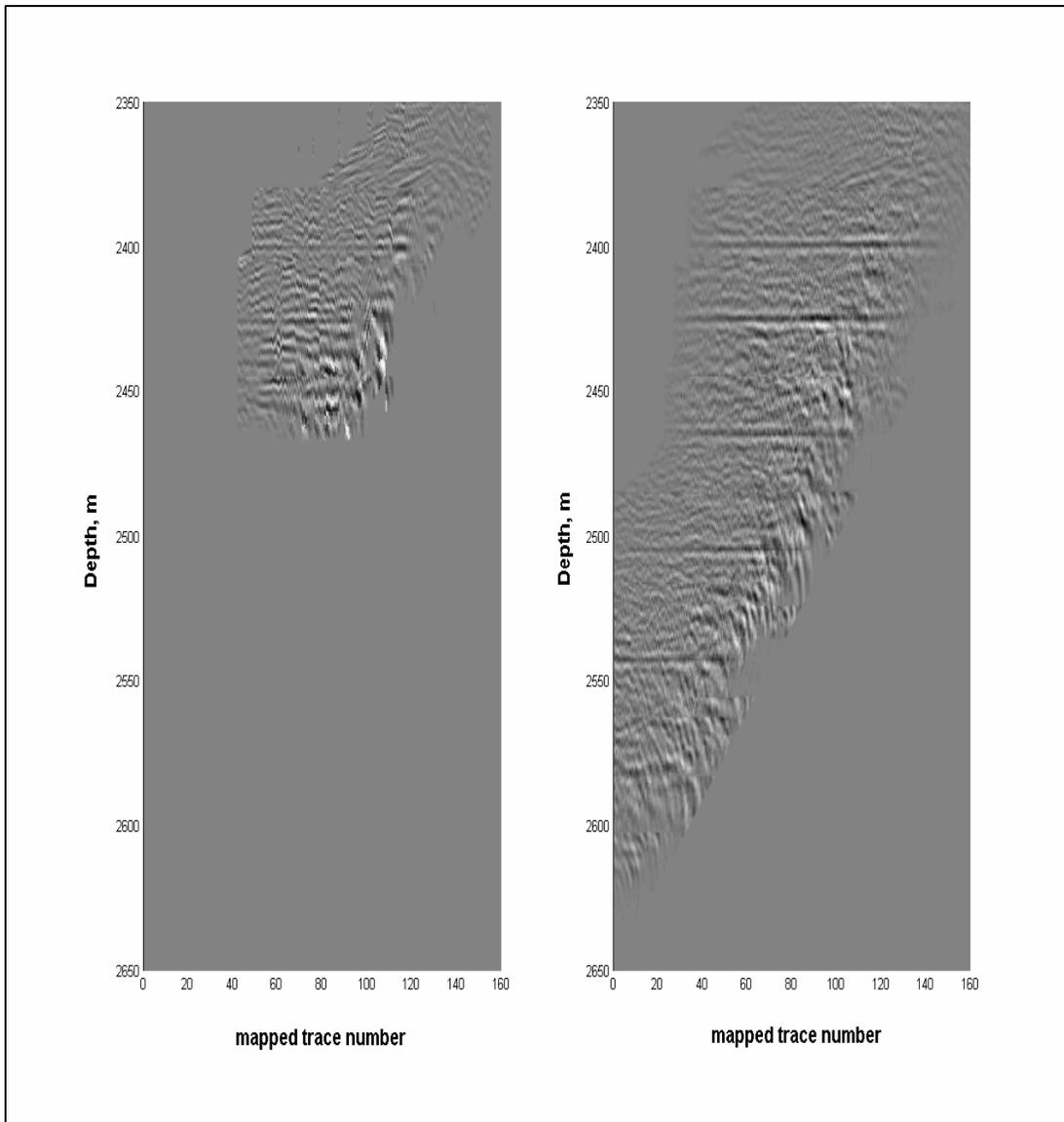
FIG. 9. Partial reflectivity maps of Figure 7 after applying residual statics corrections.

SUMMARY

We analyzed crosswell seismic data in 1.0 kHz to 1.5 kHz range from the Noel gas reservoir to create high-resolution images of the geological structure between two wells separated by about 145 m. We picked first arrival times and used a back-projection technique to create a P-wave velocity tomogram. The accuracy of the velocity tomogram was enhanced by giving due consideration to fast arrival times from head waves. The resulting tomographic velocity model would be useful for mapping hypocenters of microseismic events caused by hydraulic fracturing processes.
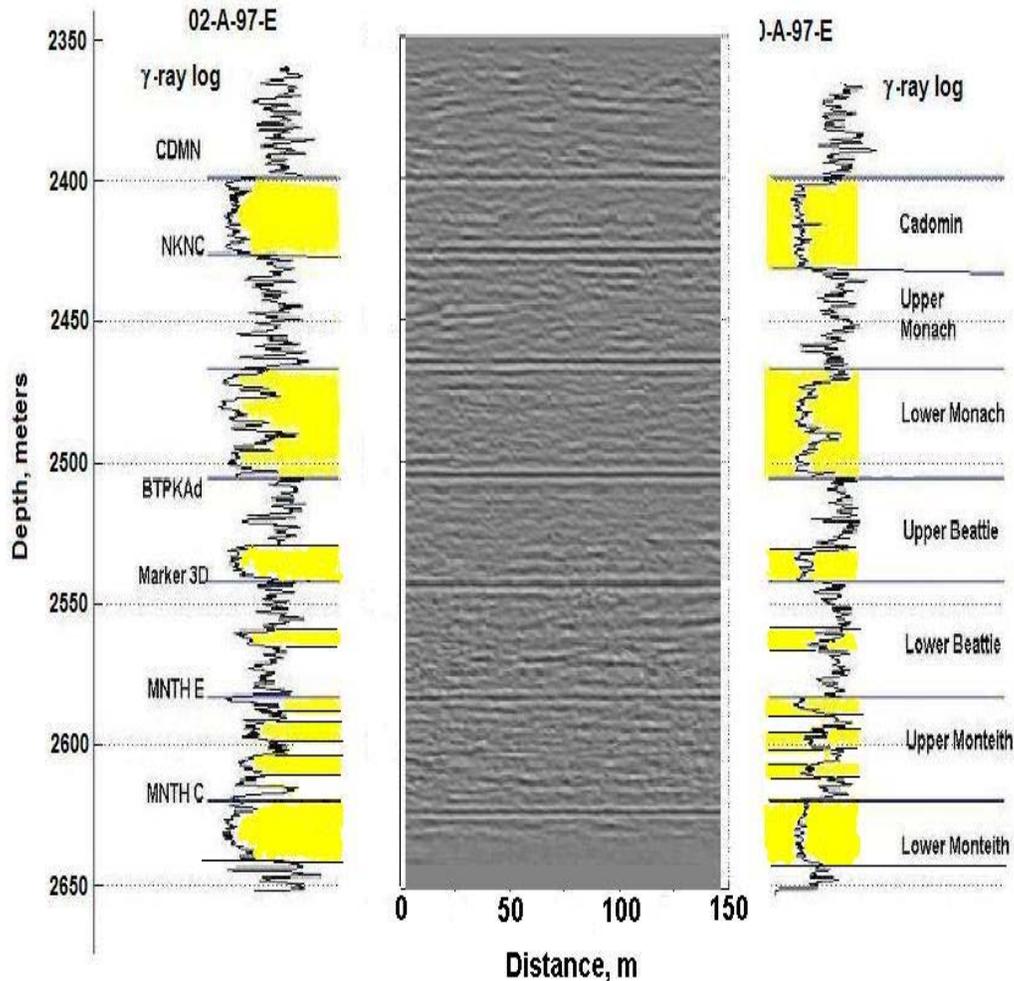
FIG. 10. Reflectivity map created from the Noel crosswell data.

We used the velocity tomogram as a guide to devise a horizontal-layer model for Snell's Law ray-tracing. This procedure gave time and geometric information for VSP/CDP mapping of up-going and down-going reflections. Although a presumably good velocity model was used to find reflection points in space, it is generally the case that statics corrections must be applied to align the mapped reflections before they stack properly (Lazaratos et al., 1995). This is especially true when the true velocity structure is complex, and/or when we have high-frequency, short-wavelength data. The short wavelengths (4 m to 6 m) and tight depth sampling intervals (.75 m to 1.5 m) used in acquiring the crosswell dataset enabled us to create a high-resolution reflectivity image.

The seismic boundaries on both the velocity tomogram and the reflectivity map show good continuity across the rock section between the wells. They correlate well with the geological layers intersected by the wells, and with the geophysical logs. The resolution on the reflectivity map is on the order of 5m to 10m, consistent with the dominant frequency (1.0 kHz to 1.5 kHz) and wavelengths in the seismic data. Tomogram P-wave velocities are in the 5.8 to 6.1 km/s range for the sandstones of the Cadomin, Lower

Monach, and Monteith geological units, and in the range 5.2 to 5.5 km/s for the shales and siltstones. These velocity values are higher than those calculated from the sonic logs transit times (5.3 to 5.6 km/s for sandstones, and 4.5 to 5.0 km/s for shales). Crosswell velocities are measured essentially in the horizontal direction, while sonic logging velocities are measured in the vertical direction. That the sonic velocities are slower than the crosswell velocities may be an indication of anisotropy.

ACKNOWLEDGEMENTS

REFERENCES

Harris, J.M., Nolen-Hoeksema, R.C., Langan, R.T., Van Schaack, M., Lazaratos, S.K., and Rector, J.W., 1995, High-resolution crosswell imaging of a west Texas carbonate reservoir: Part 1-Project summary and interpretation: Geophysics, **60**, 667-681.

Khalil, A.A., Stewart, R.R., and Henley, D.C., 1993, Full-waveform processing and interpretation of kilohertz crosswell seismic data: Geophysics, **58**, 1248-1256.

Lazaratos, S.K., Harris, J.M., Rector, J.W., and Van Schaack, M.A., 1995, High resolution crosswell imaging of a west Texas carbonate reservoir: Part 4-Reflection imaging: Geophysics, **60**, 702-711.

Li, G., and Stewart, R.R., 1996. Crosswell seismic imaging: Friendswood Texas data: J. Seismic. Expl., **5**, 323-340.

Peterson, J.E., Paulsson, B.N.P., and McEvilly, T.V., 1985, Application of algebraic reconstruction techniques to Crosshole seismic data: Geophysics, **50**, 1566-1580.

Stewart, R.R., and Marchsio, G., 1991, Crosswell seismic imaging using reflections: 61st Ann. Internat. Mtg., Soc. Expl. Geophys., Expanded Abstracts, 375-378.

Wong, J., Bregman, N., Hurley, P., and West G.F., 1987, Crosshole seismic tomography: The Leading Edge, **6**, 36-41.

Wyatt, D.K., and Wyatt, S.B., 1984, Determining subsurface structure using the vertical seismic profile, in, Vertical Seismic Profiling Part B: Advanced Concepts, Toksoz, M.N., and Stewart, R.R., ed., Geophysical Press.